Role of cardiolipin in proton transmembrane flux and localization

Sylvain Domitin, Nicolas Puff, Fanny Pilot-Storck, Laurent Tiret, Frederic Joubert

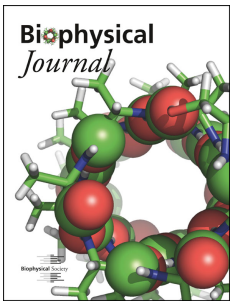

Role of cardiolipin in proton transmembrane flux and localization

Sylvain Domitin, Nicolas Puff, Fanny Pilot-Storck, Laurent Tiret, Frederic Joubert

PII: S0006-3495(24)04076-1

DOI: https://doi.org/10.1016/j.bpj.2024.12.015

Reference: BPJ 13513

To appear in: *Biophysical Journal*

Received Date: 28 May 2024

Accepted Date: 10 December 2024

Please cite this article as: Domitin S, Puff N, Pilot-Storck F, Tiret L, Joubert F, Role of cardiolipin in proton transmembrane flux and localization, *Biophysical Journal* (2025), doi: https://doi.org/10.1016/j.bpj.2024.12.015.

Manuscript submitted to **Biophysical***Journal*
Article

Role of cardiolipin in proton transmembrane flux and localization

Sylvain Domitin[1], Nicolas Puff[2,3], Fanny Pilot-Storck[4,5,6,7], Laurent Tiret[4,5,6], and Frederic Joubert[1*]

[1]Laboratoire Jean Perrin, CNRS, Sorbonne Université, UMR 8237, F-75005 Paris, France
[2]Faculté des Sciences et Ingénierie, Sorbonne Université, UFR 925 Physics, F-75005 Paris, France
[3]Laboratoire Matière et Systèmes Complexes (MSC), UMR 7057 CNRS,Université Paris Cité, F-75013 Paris, France
[4]Univ Paris-Est Créteil, INSERM, IMRB, Team Relaix, F-94010 Créteil, France
[5]École nationale vétérinaire d'Alfort, IMRB, F-94700 Maisons-Alfort, France
[6]EFS, IMRB, F-94010 Créteil, France
[7]Present address: VetAgro Sup, Campus vétérinaire, F-69280 Marcy-l'Etoile, France
[*]Correspondence: frederic.joubert@sorbonne-universite.fr

ABSTRACT In eukaryotic cells, the phospholipid cardiolipin (CL) is a crucial component that influences the function and organization of the mitochondrial inner membrane. In this study, we examined its potential role in passive proton transmembrane flux using unilamellar vesicles composed of natural egg phosphatidylcholine (PC) alone or with the inclusion of 18 or 34 mol% CL. A membrane potential was induced by a potassium gradient, and oxonol VI dye was used to monitor membrane potential dissipation resulting from proton transmembrane efflux. Increasing the CL content led to a net increase in proton efflux, which was also dependent on the magnitude of the membrane potential. The same increase in proton efflux was measured in the presence of the equally negatively charged phosphatidylglycerol (PG), indicating that the charge of CL plays a more important role than its structure in this mechanism. When varying the proton membrane permeability (p_H) using the protonophore CCCP, we observed that unlike PC liposomes, where a small amount of CCCP was sufficient to achieve maximum flux, a significantly larger amount of protonophore was required in the presence of CL. Conversely, increasing the buffer capacity increased proton flux, indicating that proton availability, rather than membrane permeability, may be the limiting factor for proton leak. Our findings demonstrated that a higher proton content associated with the membrane was correlated with an increasing leak in the presence of CL. Additionally, smaller liposome diameters appeared to favor proton leak. Taken together, our results suggest that the presence of negatively charged CL in a membrane traps protons and increases their leakage, potentially in a manner dependent on membrane curvature. We discuss possible mechanisms and implications of these findings for mitochondrial respiration function.

SIGNIFICANCE The aim of this work was to investigate the role of cardiolipin in proton transmembrane flux in the presence of a membrane potential. We observed that CL led to an increased proton leak and accumulation near the membrane, possibly favored by a higher membrane curvature. These findings confirm and refine the possible role of CL in mitochondrial function by regulating proton flux and localization.

INTRODUCTION

Biological membranes and their composition are essential for maintaining cellular functions. In mitochondria, the integrity and folding of the mitochondrial inner membrane (MIM) into cristae are crucial for the proper functioning of the respiratory chain (1–5). Alterations in lipid composition can lead to structural and functional disorders, as observed in Barth syndrome. This condition is molecularly characterized by a genetic deficiency in the proper production of cardiolipin (CL), a key phospholipid in mitochondria (6, 7).

CL are the main negatively charged phospholipids that are only found in mitochondrial membrane in eucaryote cells (8). These nonbilayer phospholipids play various roles in mitochondrial structure and function (9). Recently, we identified in mice that a

50% genetic reduction in CL content induces mitochondrial cristae dilatation and impairs the coupling efficiency of oxidative phosphorylation (OXPHOS), leading to reduced ATP production (10). We thus hypothesized that CL could enhance proton availability within the membrane, facilitating proton transfer to ATP synthase due to their negative charge and close interaction with ATPsynthase (11, 12). Several studies have also shown that CL levels influence state 4 of mitochondria respiration (13). Within membranes, CL are known to preferentially migrate to areas of strong curvature, such as mitochondrial cristae (14). They also preferentially partition into the inner leaflet of liposomes (15), and thus possibly on the MIM leaflet facing the intermembrane space (16). The presence of CL in a membrane can induce dynamic cristae-like membrane invaginations in the presence of a proton flux, thus participating in the modulation of its structure (17–19). Therefore, presence of CL could influence membrane morphology and ATP production by modulating membrane proton leak or availability, as suggested several decades ago (13). Thus, CL can play a unique role in mitochondrial function.

There is no consensus in the literature regarding the correlation between lipid composition and passive membrane permeability, especially in the presence of CL. CL is highly enriched in the MIM, where the formation of a proton gradient is a crucial step in OXPHOS. Lipid composition of the MIM is thus expected to be optimized to limit proton leakage. Due to its conical shape, CL can form non-bilayer structures (20), which could instead increase membrane permeability (21). Accordingly, the addition of CL in isolated mitochondria leads to a significant increase in proton leak and a parallel increase in respiratory rate in state 4 (22). Additionally, bilayer hydration may be modified by negative charges of the polar CL heads. Using small unilamelar vesicles (SUV), it was demonstrated in 2001 that CL could increase proton permeability, possibly by enhancing bilayer surface hydration (23). To our knowledge, no other experimental study has been conducted to evaluate the effect of CL on proton membrane permeability.

We decided to carry out a replicative analysis of this single study by conducting complementary experiments on large unilamellar vesicles (LUV), with a lipid composition mimicking that of MIM. By varying the amount of CL in a PC environment, we analyzed proton efflux following the generation of a membrane potential. Our results demonstrate that the presence of CL increases proton leak in a dose-dependent manner when a membrane potential is present, due to an increased proton concentration near the membrane. Furthermore, we propose that membrane curvature could also play a role by recruiting more CL to the inner leaflet of the membrane. These findings suggest that CL promotes proton enrichment near the membrane, potentially in a curvature-dependent manner, with significant implications for mitochondrial function.

MATERIALS AND METHODS

Chemicals

All reagents, including salts, buffers, oxonol VI fluorescent dye and lipids (bovine heart cardiolipin (CL), C0563; egg phosphatidylcholine (PC), 840051P; egg phosphatidylglycerol (PG), 841138P) were purchased from Sigma/Merck (KGaA, Darmstadt, Germany). Deionized water was used for all experiments.

Experiments on LUV in Spectrofluorometer

Preparation of LUV

Large Unilamellar Vesicles (LUV) were prepared using an extrusion technique. Natural lipids - eggPC (PC), eggPG (PG) and cardiolipin (CL) from bovine heart mitochondria (mainly 18:2 fatty acid), were used in this study. All lipids were prepared in a mixture of Chloroform/Methanol (5:3, v/v). Then 5 µmoles of different lipid mixtures (PC, PC/CL, 82:18 and 66:34 in moles, or PC/PG, 64:36) were dried by evaporation to a thin film in a round-bottomed tube under a nitrogen stream, followed by 1h under vacuum to remove residual solvent. Multilamellar liposomes were obtained by re-suspending lipids in 1 ml of a medium I (final concentration 5 mg/ml) containing 50 mM Na_2SO_4, 0.025 mM K_2SO_4, 7.5 mM Hepes, 5 mM Imidazole, pH 7.2 at 25 °C. In some experiments, ionic strength or buffer capacity were varied by adjusting Na_2SO_4 and both Hepes and Imidazole concentrations. The preparations were kept 30 min at room temperature, then vortexed 30 s before being extruded 19 times (Avanti's Mini-extruder) through polycarbonate filters (400 and then 100 nm). In some experiments, 200 nm or 50 nm filters were also used in the second extrusion to vary LUV diameter. For the lipid compositions studied, the extrusion conditions used, except for the one involving the large pore (400 nm), are expected to predominantly produce unilamellar vesicles as demonstrated by previous studies using techniques such as cryo-TEM (15, 24–26). The vast majority of experiments were carried out during the day (usually starting 30 min after extrusion), sometimes the following morning, i.e., in a maximum of 24 h. In addition, we carefully checked the reproducibility of the obtained results. Liposomes were kept in the refrigerator until use. Dynamic Light Scattering (DLS) experiments were performed to measure the mean diameter of the prepared liposomes using the Zetasizer Nano ZS (Malvern Panalytical Ltd., Grovewood, UK). All DLS data were collected using 178° backward scattering and averaged over four experimental runs, each of which was summed up over twelve-time correlograms fitted by the

Zetasizer software. The DLS values are given in Supplementary Information (SI).

Principle of membrane proton leak experiments

The experiments were based on inducting a proton efflux from LUV membranes by imposing a K^+ gradient in the presence of the K^+ transporter valinomycin, which creates a positive membrane potential E_m (excess positive charge inside) given by the Nernst equation:

$$E_m = \left(\frac{RT}{F}\right).ln\left(\frac{[K^+]_o}{[K^+]_i}\right) \quad (1)$$

where $[K^+]_i$ and $[K^+]_o$ are the potassium concentrations inside and outside the liposomes, respectively, E_m the membrane potential (in V), R the ideal gas constant (= 8.314 J.mol^{-1}.K^{-1}), T the temperature (K) and F the Faraday's constant (= 96485 C.mol^{-1}). All the experiments were performed at 25 °C. Most of the time, we added 20 mM K^+ outside the liposomes (10mM K_2SO_4), which, according to relation (1), formed an Nernst potential of 153 mV. Initially, K^+ ions alone contribute to the membrane potential.

Due to the low permeability of most ions present in the solution, only H^+ efflux is able to dissipate membrane potential (permeability in the order of 10^{-6} m.s^{-1} compared to other ions : 10^{-12}-10^{-14} m.s^{-1} for K^+ and Na^+, respectively; see (27)). Thus, the rate of the progressive decrease of membrane potential gives access to an estimation of the proton flux and ultimately proton membrane permeability. The addition of valinomycin ensured that efflux of H^+ was stoichiometrically compensated by an influx of K^+. The experiments were performed in a spectrofluorimeter (Aminco Bowman Series 2) using the fluorescent membrane potential dye oxonol VI (see Figure 1). Oxonol VI (hereafter named oxonol) is a negatively charged component that has been used in several studies (28, 29). Prepared in DMSO, oxonol is highly permeable to lipid membranes and therefore generates no potential across them, especially when used at a low concentration (29). However, the formation of a positive membrane potential induces the accumulation of this negatively charged probe in the aqueous intravesicular medium which increases the adsorption of oxonol dye on the internal leaflet of the vesicle. When the dye interacts with the lipids, it leads to a red-shift in its excitation and emission spectra, and a further red-shift occurs when a inside-positive membrane potential is generated (see oxonol spectra in (28)). Under our experimental conditions, oxonol fluorescence was measured at excitation/emission wavelengths of 618/641 nm.

The ratio of liposome to dye concentration is critical. In preliminary experiments, we observed that the maximal dynamics of the oxonol dye was obtained for very low concentrations, so we adjusted oxonol and LUV concentration to the optimal [Oxonol] = 50 nM and [LUV] = 10 μg/ml (see (28, 29)). Typical experiments for the PC and PC/CL 18 mol% conditions are shown in Figure 1: in a cuvette containing 2 ml of the solution I (with stirring and temperature control), we added 50 nM of oxonol, then LUV (10 µg/ml) and valinomycin (2 pM). External K^+ (20 mM) was finally added, creating a rapid increase of the oxonol signal. Progressive dissipation of the potential was observed, related to the efflux of H^+ and the entry of K^+. Finally, the protonophore CCCP (1 µM) was added at the end to accelerate membrane potential dissipation. Due to the negative charges of CL, the yield of oxonol partition on the membranes was decreased, leading to a smaller response of the dye after LUV addition and membrane potential formation. Calibration of experiments conducted with oxonol (see below) was performed, allowing us to compare the membrane potential responses for the different lipid mixtures used.

In multilamellar vesicles (non-extruded LUV), all the kinetics were greatly reduced (see Supplementary Information (SI)): the oxonol response to LUV addition was slowed down, as well as after K^+ and CCCP addition. The maximal membrane potential was also decreased, and no significant proton efflux occurred. Based on these data, less than 5% samples with slow kinetics were considered as poorly extruded and were further discarded from the analysis. Finally, we verified that in the presence of valinomycin, the addition of K_2SO_4 induced no significant liposome shrinkage associated to the hypertonic osmotic shock (barely unchanged liposome diameters, see DLS experiments, Table S2 in Supplementary Information (SI)).

Analysis of oxonol experiments

To convert the oxonol dye fluorescence into voltage, we used the different parameters obtained in our experiments (see Figure 1), and the formalism developed in (29). Calibration of the oxonol signal was carried out for each lipid composition (Supplementary Information (SI)). This allowed to normalize data obtained from the probe on the specificity of each lipid, including the unique ratio of free versus membrane-associated molecules, strictly depending on the amount of negative charges of lipids.

Using all the detailed calibrations, the membrane potential (in V) was given by:

$$E_m = \left(\frac{RT}{F}\right).ln\left[\frac{(2R_{t_i}+1)}{1-\frac{Ox_t.(2R_{t_i}+1).(Ft_{E_m}-F_w)}{N.Lip.F_w.(R_{t_i}+1).(\phi_r-1)})}\right] \quad (2)$$

with

$$R_{t_i} = \frac{F_w.(Ft_{E_m} - Ft_o).(\phi_r - 1)}{(\phi_r.F_w - Ft_{E_m}).(Ft_0 - F_w)} \quad (3)$$

where most of the parameters are defined in Figure 1, Rt_i is the ratio ($= \frac{\Delta F}{F_0}$) of fluorescence of the oxonol VI probe corrected for depletion; Ox_t is the total concentration of oxonol in solution (μM); N is the specific number of membrane sites of oxonol (mole/mole of lipid); Lip is the lipid vesicle concentration (μM); ϕ_r is the relative fluorescence yield. The yield $\phi_r = F_{mlip}/F_w$ and the parameter $N = F_{mox}.O_{xt}/F_{mlip}.Lip$, are given by calibration experiments as explained in (29) (see SI).

Calculation of K^+ and H^+ flux

The function $E_m(t)$ was converted into volts, allowing to deduce the variation of K^+ and H^+ concentrations inside the liposomes. At an instant t, the measured potential $E_m(t)$ was considered as the difference between the positive potassium potential $E_K(t)$ given by (1) and the progressive negative proton potential $E_H(t)$ formed during oxonol experiment:

$$E_m(t) = E_K(t) - E_H(t) = \left(\frac{RT}{F}\right).ln\left(\frac{[K^+]_o}{[K^+]_i(t)}\right) - \left(\frac{RT}{F}\right).ln\left(\frac{[H^+]_o}{[H^+]_i(t)}\right)$$

$$E_m(t) = \left(\frac{RT}{F}\right).ln\left(\frac{[K^+]_o.[H^+]_i(t)}{[K^+]_i(t).[H^+]_o}\right) \quad (4)$$

$[H^+]_o$ and $[K^+]_o$ did not vary during time because of the large volume of the cuvette. To determine the variation of $[K^+]_i$ over time, we needed to establish the relationship between $[H^+]_i(t)$ and $[K^+]_i(t)$. As explain above, the presence of valinomycin ensured the instantaneous entry of a K^+ ion for each proton that left the LUV. Thus, electroneutrality was preserved and membrane dissipation occurred at quasi-equilibrium. Therefore, the amount of H^+ leaving was equal to the amount of K^+ entering, $\Delta[H^+]_i(t) = -\Delta[K^+]_i(t)$. Finally, due to the buffer capacity of the solution, the variation of internal $[H^+]_i(t)$ was related to pH variation according to the relation:

$$\Delta pH_i(t) = -\frac{\Delta[K^+]_i(t)}{\beta} \quad (5)$$

where β is the buffer capacity of the solution. So, at each time t, $[K^+]_i(t)$ and $[H^+]_i(t)$ were given by:

$$[K^+]_i(t) = [K^+]_{i0} + \Delta[K^+]_i(t) \quad (6)$$

$$[H^+]_i(t) = 10^{-(pH_{i0}+\Delta pH_i(t))} = [H^+]_{i0}.10^{-\left(\frac{\Delta[K^+]_i(t)}{\beta}\right)} \quad (7)$$

where $[K^+]_{i0}$ and $[H^+]_{i0}$ were the initial values of $[K^+]$ and $[H^+]$ at maximum E_m. $[K^+]_{i0}$ was calculated using relation (1) assuming no initial proton flux. Using the relations (4), (6) and (7), it was thus possible to obtain the following equation giving the link between $\Delta[K^+](t)$ and $E_m(t)$ at each time t:

$$\left(\frac{[H^+]_o}{[K^+]_o}\right).\left(\frac{[K^+]_{io}}{[H^+]_{io}}\right).\left(1 + \frac{\Delta[K^+]_i(t)}{[K^+]_{io}}\right).\exp\left(\frac{F}{RT}.E_m(t)\right) = 10^{-(\Delta[K^+]_i(t)/\beta)} \quad (8)$$

This equation, which is in the form of $A + BX = 10^{-(X/\beta)}$ with $X = \Delta[K^+]$ could be solved numerically for each $E_m(t)$, which allowed to obtain the variation of $[K^+]_i(t)$ and $[H^+]_i(t)$ (using a custom-written programs in MATLAB, The MathWorks; Natick, Massachusetts, United States). Using the experimental data obtained from the oxonol experiments, we were able to calculate the kinetic parameters of proton efflux.

As explained above, the fluxes of H^+ and K^+ were equivalent. We could therefore assimilate the incoming flux of K^+ to the outgoing flux of H^+ because the latter was limiting in the exchange kinetics:

$$J_H = -J_K \quad (9)$$

As a flux through a liposome of volume V is defined as the amount of ions that cross a section A of the membrane, we had $J_{K_i} = (\frac{dK_i^+}{dt}).(\frac{V}{A})$. The maximal flux $J_{H_{max}}$ could be easily calculated using the initial slope of $[K^+]_i(t)$, just after the potential jump in the curve $[K^+]_i(t)$. Finally, because of (9), the proton membrane permeability p_H could be calculated using the Nernst-Planck relationship (30):

$$J_{K_i} = -J_{H_i} = -p_H.\overline{E_{m_i}}.\frac{([H^+]_o - [H^+]_i \exp(\overline{E_{m_i}}))}{(1 - \exp(\overline{E_{m_i}}))} = -p_H.\overline{E_{m_i}}.[H^+]_o.\frac{(1 - R_i \exp(\overline{E_{m_i}}))}{(1 - \exp(\overline{E_{m_i}}))} \quad (10)$$

with p_H=permeability of H^+ ions (in m/s), $\overline{E_{m_i}} = \left(\frac{F}{RT}\right) E_{m_i}$, and $R_i = \left(\frac{[H^+]_i}{[H^+]_o}\right)$.

So p_H was given by:

$$p_H = -\frac{J_K.(1 - \exp(\overline{E_{m_i}}))}{\overline{E_{m_i}}.[H^+]_o.(1 - R_i \exp(\overline{E_{m_i}}))}. \quad (11)$$

We considered that no significant H^+ flux occurred just after the potential formation (maximal flux), meaning that initially $[H^+]_o = [H^+]_i$. Equation (10) could then be simplified:

$$J_{H_{max}} = p_H.\overline{E_{m_{max}}}[H^+]_o \quad (12)$$

and the proton permeability was obtained by:

$$p_H = \frac{J_{H_{max}}}{\overline{E_{m_{max}}}.10^{-pH}} \quad (13)$$

RESULTS

CL increase proton efflux in LUV

To study how the presence of CL modifies proton passive transmembrane flux, we generated 100 nm diameter liposomes containing PC or a mix of PC/CL (82/18 and 66/34 in moles) and using the oxonol dye, measured proton efflux after the formation of a membrane potential. The formalism developed by the Pouliquin's paper (29) (equations (2-3) and Figure 1) was used to convert the oxonol signal in mV. After the addition of 20 mM of K^+ outside the LUV, a positive membrane potential was rapidly created (Figure 2A), although it was lower than the theoretical one given by the equation (1). The difference was attributed to the presence of a high membrane capacitance (for details, see (28, 29)). After a few minutes, this membrane potential dissipated, indicating an efflux of protons. The addition of CCCP, a membrane protonophore, accelerated this dissipation, confirming the involvement of protons (Figure 2A).

The initial maximum potential reached in the three conditions of LUV composition differed significantly: in the presence of increasing level of CL, $E_{m_{max}}$ was significantly lower than with PC alone (Figure 2A and Table 1). This could be related to an increase in proton leak and an experimental mixing time (around 3 s) that did not allow precise estimation of the initial E_m (see below). The potential dissipation also appeared to be faster. To estimate proton leak and permeability coefficient, we used the Nernst-Planck relation and the equations (8-13). This provided the variation of $[K^+]$ and $[H^+]$ during membrane potential dissipation (Figure 2B), and allowed estimation of maximal flux (at maximal E_m) and proton permeability using equation (13). Results are presented in Table 1. The near doubling of CL content led to a marked increase in proton leakage and membrane permeability to protons. Thus, the presence of CL in a PC membrane increased proton permeability in a dose-dependent manner.

To assess the relative impact of CL charges on this efflux, we carried out the same experiment replacing CL with phosphatidylglycerol (PG), also negatively charged. As CL structure corresponds approximately to two PG molecules, we prepared a 36% molar PC/PG lipid mixture. The kinetic parameters of proton efflux obtained with the 36 mol% PC/PG mixture were identical to those obtained with the 18 mol% PC/CL mixture (Table 1 and Supplementary Information (SI)), supporting the hypothesis that in our experiments, the negative charges of CL mostly contributed to the increased proton efflux.

Table 1: Kinetic parameters of membrane potential experiments

	Membrane Potential (mV)	Maximal Flux (nmole/s/m^2)	Permeability (μm/s)
PC	103 (2)	0.148 (0.013)	0.60 (0.07)
PC/CL 18 mol%	91 (2) **	0.234 (0.015) **	1.05 (0.07) **
PC/CL 34 mol%	80 (4) $^{\$}$	0.381 (0.012) $^{\$\$}$	1.93 (0.07) $^{\$\$}$
PC/PG 36 mol%	88 (1) *	0.225 (0.006) *	1.03 (0.03) **

Results are given in Mean (S.E.M.) (n = 16 experiments for PC and PC/CL 18 mol%; n = 6 for PC/CL 34 mol% and PC/PG 36 mol%). t-Student test : PC vs PC/CL 18 mol% or PC/PG 36 mol%: * p<0.01, ** p<0.001; PC/CL 18 mol% vs PC/CL 34 mol%: $^{\$}$ p<0.05, $^{\$\$}$ p<0.005. No significant difference was observed between PC/CL 18 mol% and PC/PG 36 mol% lipid mixtures.

CL-dependent proton flux is positively correlated with membrane potential

The Nernst-Planck relationship (10) and equation (12) predict that if no H^+ net efflux occurs after the generation of a membrane potential, the initial maximum proton leak must be proportional to the membrane potential, proton permeability and H^+ concentration. Thus, for a given H^+ concentration, variations of the initial membrane potential allow to estimate the permeability by an alternative method, i.e. through the slope of the Flux = f(E_m) relationship. This calculation was used to confirm an influence of CL content on proton flux. We varied the gradient of K^+ imposed on the membrane by changing the concentration of $[K^+]_{out}$ injected in solution. Results are presented in Figure 3. As expected by the Nernst-Planck equation, the proton flux increased almost linearly with the imposed membrane potential. In these experiments, the estimation of permeability for PC and PC/CL 18 mol% yielded values of 0.80 and 1.36 μm/s respectively, which were values close to those obtained in Table 1. This confirmed that proton leak was higher in the presence of CL.

CL reduces CCCP-induced proton permeability

To check whether our measurements were in accordance with the Nernst-Planck relationship at both lipid conditions, we injected increasing amounts of the CCCP protonophore prior to membrane potential. No major change occurred (< 5%) in the fluorescence signal after CCCP addition, indicating that CCCP did not modify the interaction of oxonol dye with the membranes at the low concentrations (<20 nM) we used here. The results of the kinetic experiments are presented in Figure 4.

We first verified that $E_{m_{max}}$ decreased upon increased membrane permeability to protons. Indeed, in both lipid conditions, $E_{m_{max}}$ progressively decreased when CCCP concentration increased, and more rapidly in the presence of PC alone than with CL (Figure 4A). This strongly suggested that the previous difference observed between PC and PC/CL mixtures was due to a higher initial proton leak with CL. We also observed that both types of LUV composition influenced the estimated proton permeability. While in the presence of PC alone, 2.5 nM of CCCP was sufficient to rapidly achieve maximum proton permeability, the addition of CL to LUV required 10 times more CCCP to reach maximum permeability, with slower kinetics (Figure 4B). This behavior was also consistent with the variation of maximal membrane potential after CCCP addition: for PC, there was an initial massive drop, while for PC/CL, the maximal membrane potential slowly decreased when CCCP concentration increased. Finally, by increasing the number of charges at the membrane using PC/CL 34 mol% lipid mixture, we observed the same kinetics (Supplementary Information (SI)), suggesting that the CCCP dose-response in the presence of CL was not solely related to the level of negative charge at the membrane likely attenuating the effect of CCCP. In summary, while membrane permeability to protons played a prominent role for PC LUV, another factor prevented the fast efflux of protons through the membrane in PC LUV supplemented with CL. According to the Nernst-Planck relationships, this factor could be the availability in H^+.

CL promotes proton availability at the membrane

To test whether the amount of available protons in the presence of CL can be a limiting factor for their efflux through the membrane, we first increased the global reserve of protons by elevating the buffering capacity of the solution both for PC and PC/CL 18 mol% LUV. Accordingly, proton efflux increased linearly with buffering capacity, but stayed higher in PC/CL 18 mol% LUV compared to PC LUV (Figure 5A).

Alternatively, the increased proton fluxes observed for CL-enriched membrane could result from the very local concentration of protons in the vicinity of the internal leaflet of the membrane. In this case, we hypothesized that, in the presence of CL, increasing the ionic strength of the solution would shield the negative charges on the membrane, reduce the proton concentration - due to the presence of other ions, and thereby decrease proton leak. Accordingly, we quantified that after a 4-fold increase in the ionic strength of internal and external solutions, no change occurred for PC alone LUV, whereas the previously observed decrease of the membrane potential and increase of proton efflux in LUV enriched with CL (Figure 2) was normalized and reached values similar to those in LUV without CL (Figure 5B). This result strongly suggests that charges carried by CL act as proton antenna and create a larger reserve of protons at the membrane, responsible for the increase of proton flux. It also means that in the presence of CL, the local $[H^+]$ has to be used in the Nernst-Planck relationship. A calculation shows that if p_H is identical without or with CL, it means that local pH is acidified and shift by -0.2 and -0.4 in the presence of 18 and 34 mol% of CL respectively (using data from Table 1).

Proton permeability and LUV curvature

It has been shown that depending on curvature, CL sorting can occur (14). According to this hypothesis, more CL is expected to be present in the inner leaflet of smaller-sized LUV, which should lead to increased proton leak in the smallest LUV. To address the putative influence of membrane curvature on proton fluxes in the presence of CL, we varied the size of LUV from 450 nm to 80 nm depending on the lipid mixture (Figure 5). In the presence of PC alone, proton permeability was globally insensitive to

LUV diameter. On the contrary, we observed a trend towards increased membrane proton permeability for CL-enriched LUV as the size of LUV decreased. The apparent reduction in permeability observed for LUV extruded with the 400 nm pore filter could likely be attributed to the higher presence of multilamellar vesicles, but this was not the case for other conditions (see Figure S5 in SI). Although we were technically limited from reducing the diameter below 80 nm, this result is consistent with the mechanistic hypothesis of local proton enrichment at the membrane level in the presence of CL.

DISCUSSION

The main objective of this study was to elucidate how the presence of cardiolipins (CL) influences proton flux across a lipid membrane and to underscore a potential connection between membrane lipid composition, morphology, and ion exchanges across it. This issue is crucial in the context of the highly curved mitochondrial cristae, where the proton gradient generated by the respiratory chain is maintained and regulated to facilitate ATP production. Here, we demonstrated that CL play a pivotal role in the efflux of H^+ across the membrane of LUV. At 25 °C, an 18 mol% CL content in the lipid composition of the membrane (partially representative of the mitochondrial inner membrane composition) was sufficient to increase the efflux of protons and the permeability to these protons by 1.5-fold. As the percentage of CL increased, the proton efflux continued to rise. Moreover, the increase in proton efflux in the presence of CL was observed regardless of the applied potential. These results indicate that the presence of CL increases proton efflux, confirming previous data obtained on liposomes (23). They contradict the "protective" role of CL sometimes suggested in the literature (31). We also show that the negative charges of CL represent the major parameter by which they contribute to this increase in proton efflux. Our results confirm the involvement of CL in the regulation of proton leak, and thus potentially in mitochondrial respiration in state 4, initially based on the identification more than 20 years ago of a positive correlation between passive proton leakage in state 4 and the amount and type of CL in mitochondria (13).

To understand how the presence of CL influences proton efflux in the presence of a membrane potential, we performed several experiments. i) We initially increased proton permeability by increasing doses of the CCCP protonophore. With PC alone, maximal proton efflux was reached at 2.5 nM CCCP, whereas in the presence of CL, proton efflux progressively increased and reached its maximum at much higher CCCP concentrations. This may indicate that membrane proton permeability is not a limiting factor for proton flux in the presence of CL. Of note, we cannot totally exclude that the negative charges of CCCP partially reduced the efficiency of its interaction with CL-containing membranes. However, the lipophilic properties of CCCP, and the experiment performed by doubling the amount of CL (Figure S4) suggest that the CCCP dose-response is not solely related to the level of negative charges at the membrane. ii) According to the Nernst-Planck relationship, proton efflux also relies on the concentration of H^+ near the membrane. Therefore, we varied the amount of H^+ available in our solution by modulating its buffering capacity. These experiments revealed that a higher buffering capacity increased proton flux for both PC and PC/CL conditions, but did not explain the higher flux in the presence of CL. iii) In parallel, we investigated whether a higher localization of protons at the membrane was responsible for the increased proton efflux in the presence of CL. Due to its negative charge at physiological pH, CL can act as a "proton antenna" (13, 32). To explore this, we varied the ionic strength of the solution: at very high ionic strength (600 mM), most of the membrane charges are probably shielded and the PC/CL LUV are expected to contain less protons within the membrane. Our experiments supported this hypothesis: at high ionic strength, the membrane permeability to protons with and without CL became very similar. This suggests that the negative charges of CL play an important role in proton efflux across the membrane by creating a larger proton reserve than PC alone in the membranes, eventually facilitating proton efflux. This finding is consistent with previous data reporting a more acidic pH of membranes containing CL (33). Using our data, we calculated a local pH shift of -0.2 and -0.4 in the presence of 18 and 34 mol% of CL respectively. iv) In a final series of experiments, we investigated how membrane curvature may affect proton efflux in the presence of CL. When increasing membrane curvature by decreasing LUV diameter, we observed a tendency for apparent proton permeability to increase in the presence of CL. This is in line with recent studies showing induced sorting of CL upon increased membrane curvature, and CL partition to the inner leaflet of 100 nm vesicles (14, 15). Our results support the mechanistic hypothesis by Elmer-Dixon and colleagues who proposed that curvature-based sorting results from lipid-lipid interactions (15). The apparent reduction in permeability calculated for LUV extruded with the 400 nm pore filter could be attributed to the greater number of multilamellar vesicles in this condition, as shown in the past (26). Here, we demonstrated that increasing CL content in the membrane from 18% to 34% doubled proton efflux and the calculated permeability (Table 1), suggesting that a threshold value of curvature must be reached to induce CL sorting and produce a significant effect on proton efflux. The role of CL enrichment in achieving higher curvature values approaching those of mitochondrial cristae, thus yielding elevated proton efflux, is an exciting avenue for the present work. In this respect, the experimental approach developed by Beltrand-Heredia and collaborators should be an option to consider (14). Our finding has interesting consequences, since mitochondrial cristae are dynamic structures of 10-20 nm diameter that change their shape according to the energy demand and mitochondrial activity (34). In state 4 (condensed shape), the maximum curvature would correspond to a situation of

increased proton leak without impairing OXPHOS efficiency because no ATP is formed; in state 3 (orthodox shape), membrane curvature is reduced, which would prevent proton leak and preserve OXPHOS efficiency to produce ATP by consuming the proton gradient. By allowing fine-tuning of membrane shape, proton leak and ATP formation, the presence of CL would thus participate in the regulation of mitochondrial activity (19). The role of CL in the cellular response to fluctuating ATP needs could also be indirect, via its interaction with numerous proteins, such as cytochrome c, whose release from the mitochondria coincides with cristae remodeling and initiation of the apoptosis process. Finally, in mitochondrial cristae that include the additional presence of the ATP synthase, we can further speculate that proton trapping by CL may constitute a reservoir of protons available to cross the ATP synthase and generate the proton-motive force. This hypothesis is supported by the reduced OXPHOS coupling efficiency observed in muscles of *Hacd1*-KO mice characterized by a 2-fold reduction in their mitochondria CL content (10).

CONCLUSION

In this study, using *in vitro* LUV experiments, we showed that in the presence of a membrane potential, cardiolipin (CL) increases proton efflux, likely by compartmentalizing protons along the membrane. This phenomenon may be exacerbated by higher membrane curvatures, which increase CL recruitment to the inner leaflet of the membrane. These findings have important consequences for mitochondrial cristae structure and functions, suggesting that the negative charge and its affinity for curved areas play a direct role in modulating mitochondrial activity. Thus, our study provides key insights into the link established by CL between mitochondrial membrane morphology and mitochondrial activity. Adjusting the amount of CL on the inner leaflet depending on mitochondrial cristae curvature would modify the locally available amount of H^+ and as a result, the OXPHOS coupling efficiency for demand-driven ATP production. Further experiments including the addition of ATP synthase in membrane systems are warranted to confirm the ability of CL to facilitate proton membrane diffusion towards the ATP synthase, and to quantify the balance between the dual promotion of proton leakage and proton channeling by CL.

AUTHOR CONTRIBUTIONS

All authors conceptualized and designed the study. S.D. and F.J. performed the experiments and analyzed the data. All authors discussed the results and implications, and contributed to the writing and editing of the manuscript, as well as to the reviewing process.

ACKNOWLEDGMENTS

Biological studies in mice, which led to the formulation of the hypotheses developed in this article, were partly funded by the "Association Française contre les Myopathies" (AFM 16143, Translamuscle I (19507) and Translamuscle II (22946)).

DECLARATION OF INTERESTS

The authors declare no competing interests.

REFERENCES

1. Zick, M., R. Rabl, and A. S. Reichert, 2009. Cristae formation—linking ultrastructure and function of mitochondria. *Biochimica et Biophysica Acta (BBA) - Molecular Cell Research* 1793:5–19.

2. Cogliati, S., J. A. Enriquez, and L. Scorrano, 2016. Mitochondrial Cristae: Where Beauty Meets Functionality. *Trends in Biochemical Sciences* 41:261–273.

3. Glancy, B., Y. Kim, P. Katti, and T. B. Willingham, 2020. The Functional Impact of Mitochondrial Structure Across Subcellular Scales. *Frontiers in Physiology* 11:1462.

4. Colina-Tenorio, L., P. Horten, N. Pfanner, and H. Rampelt, 2020. Shaping the mitochondrial inner membrane in health and disease. *Journal of Internal Medicine* 287.

5. Joubert, F., and N. Puff, 2021. Mitochondrial Cristae Architecture and Functions: Lessons from Minimal Model Systems. *Membranes (Basel)* 11.

6. Schlame, M., and M. Ren, 2006. Barth syndrome, a human disorder of cardiolipin metabolism. *FEBS Letters* 580:5450–5455.

7. Acehan, D., Y. Xu, D. Stokes, and M. Schlame, 2007. Comparison of lymphoblast mitochondria from normal subjects and patients with Barth syndrome using electron microscopic tomography. *Laboratory investigation; a journal of technical methods and pathology* 87:40–8.

8. Hoch, F. L., 1992. Cardiolipins and biomembrane function. *Biochimica et Biophysica Acta (BBA) - Reviews on Biomembranes* 1113:71–133.

9. Basu Ball, W., J. K. Neff, and V. M. Gohil, 2018. The role of nonbilayer phospholipids in mitochondrial structure and function. *FEBS Letters* 592:1273–1290.

10. Prola, A., J. Blondelle, A. Vandestienne, J. Piquereau, R. G. P. Denis, S. Guyot, H. Chauvin, A. Mourier, M. Maurer, C. Henry, N. Khadhraoui, C. Gallerne, T. Molinié, G. Courtin, L. Guillaud, M. Gressette, A. Solgadi, F. Dumont, J. Castel, J. Ternacle, J. Demarquoy, A. Malgoyre, N. Koulmann, G. Derumeaux, M.-F. Giraud, F. Joubert, V. Veksler, S. Luquet, F. Relaix, L. Tiret, and F. Pilot-Storck, 2021. Cardiolipin content controls mitochondrial coupling and energetic efficiency in muscle. *Science Advances* 7.

11. Duncan, A. L., A. J. Robinson, and J. E. Walker, 2016. Cardiolipin binds selectively but transiently to conserved lysine residues in the rotor of metazoan ATP synthases. *Proc Natl Acad Sci U S A* 113:8687–8692.

12. Mühleip, A., S. E. McComas, and A. Amunts, 2019. Structure of a mitochondrial ATP synthase with bound native cardiolipin. *Elife* 8.

13. Hoch, F. L., 1998. Cardiolipins and mitochondrial proton-selective leakage. *J Bioenerg Biomembr* 30:511–532.

14. Beltrán-Heredia, E., F.-C. Tsai, S. Salinas-Almaguer, F. J. Cao, P. Bassereau, and F. Monroy, 2019. Membrane curvature induces cardiolipin sorting. *Communications Biology* 2:225.

15. Elmer-Dixon, M. M., J. Hoody, H. B. B. Steele, D. C. Becht, and B. E. Bowler, 2019. Cardiolipin Preferentially Partitions to the Inner Leaflet of Mixed Lipid Large Unilamellar Vesicles. *The Journal of Physical Chemistry B* 123:9111–9122.

16. Golla, V. K., K. J. Boyd, and E. R. May, 2024. Curvature sensing lipid dynamics in a mitochondrial inner membrane model. *Communications Biology* 7:29.

17. Khalifat, N., N. Puff, S. Bonneau, J.-B. Fournier, and M. I. Angelova, 2008. Membrane Deformation under Local pH Gradient: Mimicking Mitochondrial Cristae Dynamics. *Biophysical Journal* 95:4924–4933.

18. Khalifat, N., J.-B. Fournier, M. I. Angelova, and N. Puff, 2011. Lipid packing variations induced by pH in cardiolipin-containing bilayers: The driving force for the cristae-like shape instability. *Biochimica et Biophysica Acta (BBA) - Biomembranes* 1808:2724–2733.

19. Patil, N., S. Bonneau, F. Joubert, A.-F. Bitbol, and H. Berthoumieux, 2020. Mitochondrial cristae modeled as an out-of-equilibrium membrane driven by a proton field. *Phys. Rev. E* 102:022401.

20. Rand, R., and S. Sengupta, 1972. Cardiolipin forms hexagonal structures with divalent cations. *Biochimica et Biophysica Acta (BBA) - Biomembranes* 255:484–492.

21. Gasanov, S. E., A. A. Kim, L. S. Yaguzhinsky, and R. K. Dagda, 2018. Non-bilayer structures in mitochondrial membranes regulate ATP synthase activity. *Biochimica et Biophysica Acta (BBA) - Biomembranes* 1860:586–599.

22. Bobyleva, V., M. Bellei, T. L. Pazienza, and U. Muscatello, 1997. Effect of cardiolipin on functional properties of isolated rat liver mitochondria. *Biochem Mol Biol Int* 41:469–480.

23. Chen, Q.-P., and Q.-T. Li, 2001. Effect of Cardiolipin on Proton Permeability of Phospholipid Liposomes: The Role of Hydration at the Lipid–Water Interface. *Archives of Biochemistry and Biophysics* 389:201–206.

24. Kamal, M. M., D. Mills, M. Grzybek, and J. Howard, 2009. Measurement of the membrane curvature preference of phospholipids reveals only weak coupling between lipid shape and leaflet curvature. *Proc Natl Acad Sci U S A* 106:22245–22250.

25. Nele, V., M. N. Holme, U. Kauscher, M. R. Thomas, J. J. Doutch, and M. M. Stevens, 2019. Effect of Formulation Method, Lipid Composition, and PEGylation on Vesicle Lamellarity: A Small-Angle Neutron Scattering Study. *Langmuir* 35:6064–6074.

26. Scott, H. L., A. Skinkle, E. G. Kelley, M. N. Waxham, I. Levental, and F. A. Heberle, 2019. On the Mechanism of Bilayer Separation by Extrusion, or Why Your LUVs Are Not Really Unilamellar. *Biophys J* 117:1381–1386.

27. Paula, S., A. G. Volkov, A. N. Van Hoek, T. H. Haines, and D. W. Deamer, 1996. Permeation of protons, potassium ions, and small polar molecules through phospholipid bilayers as a function of membrane thickness. *Biophys J* 70:339–348.

28. Apell, H. J., and B. Bersch, 1987. Oxonol VI as an optical indicator for membrane potentials in lipid vesicles. *Biochim Biophys Acta* 903:480–494.

29. Pouliquin, P., J. Grouzis, and R. Gibrat, 1999. Electrophysiological study with oxonol VI of passive NO3- transport by isolated plant root plasma membrane. *Biophys J* 76:360–373.

30. STEIN, W. D., 1986. CHAPTER 1 - Physical Basis of Movement across Cell Membranes. *In* W. D. STEIN, editor, Transport and Diffusion Across Cell Membranes, Academic Press, 1–68.

31. Ikon, N., and R. O. Ryan, 2017. Barth Syndrome: Connecting Cardiolipin to Cardiomyopathy. *Lipids* 52:99–108.

32. Haines, T. H., and N. A. Dencher, 2002. Cardiolipin: a proton trap for oxidative phosphorylation. *FEBS Lett* 528:35–39.

33. Parui, P. P., Y. Sarakar, R. Majumder, S. Das, H. Yang, K. Yasuhara, and S. Hirota, 2019. Determination of proton concentration at cardiolipin-containing membrane interfaces and its relation with the peroxidase activity of cytochrome c. *Chem Sci* 10:9140–9151.

34. Hackenbrock, C. R., 1966. Ultrastructural bases for metabolically linked mechanical activity in mitochondria. I. Reversible ultrastructural changes with change in metabolic steady state in isolated liver mitochondria. *J Cell Biol* 30:269–297.

LEGEND OF THE FIGURES

...

Figure 1: Principle of the experiment. Insert: in the presence of LUV, the part of the oxonol dye (red dots) that binds to the membrane increases in the presence of a positive membrane potential due to the negative charge of oxonol VI. Typical oxonol experiments performed at 25 °C in this study for PC and PC/CL 18 mol% conditions (grey and blue curves): at t = 30 s, 50 nM of oxonol was added to the cuvette, then 10 µg/ml of LUV at t = 130 s and 2 pM of valinomycin at 200 s. A t = 260 s, 10 mM of K_2SO_4 was added to generate a membrane potential. At t = 500 s, 1 µM of the protonophore CCCP was added to completely dissipate the potential. All the parameters defined here were used to calibrate the dye using the formalism developed by Pouliquin et al. (29): F_w: fluorescence after adding oxonol to the solution I; F_{tEm}: fluorescence after the creation of the K^+ gradient at the membranes; F_{t0}: fluorescence after potential neutralization with the protonophore (CCCP); F_0: increase in fluorescence by oxonol-membrane bonds (= F_{t0} - F_w); ΔF: increase in fluorescence by the K^+ gradient, ΔF_i initially (= F_{tEm} - F_{t0}); R_t: The fluorescence ratio of the oxonol VI probe (= $\Delta F / F_0$).

Figure 2: A. Influence of cardiolipin amount on proton efflux. Time dissipation of membrane potential calibrated using equation (2) for the different lipid mixtures (PC alone, PC + 18 mol% and + 34 mol% CL). Curves are the mean of 16 experiments for PC and PC/CL 18 mol%, and six experiments for PC/ CL 34 mol% (± s.e.m.). B. Calculated $[K^+]_i$ and $[H^+]_i$ variations during membrane potential dissipation using data of Figure 2A and equation (8).

Figure 3: Proton leak measurement without and with CL 18 mol% for different membrane potentials. Different external [K_2SO_4] were used to vary membrane potential (10, 5, 1, 0.5, 0.2 mM), when internal [K_2SO_4] was kept unchanged. Estimation of permeability was obtained using relation (13) and a linear regression of the proton leak versus membrane potential relationship. (n = 16 for maximum potential, and n = 4-6 experiments for other points ± s.e.m.).

Figure 4: Effect of low doses of CCCP on initial membrane potential and permeability. Increasing doses of CCCP was added before generating a membrane potential. A. Maximal potential formed after CCCP addition without or with CL. B. Membrane permeability to proton obtained during membrane potential dissipation experiment without or with CL (n = 16 for 0 CCCP, and n = 4-6 experiments for others points, ± s.e.m.).

Figure 5: Effect of proton availability on proton efflux with or without cardiolipin. A. Variation of proton efflux depending on buffer capacity (n = 4-5 for each point). The concentration of Hepes and imidazole were progressively increased, while the Hepes/imidazole ratio was kept constant (1.5). B. Variation of initial membrane potential and proton efflux in response to a 4-fold increase in ionic strength (150 to 600 mM) (n = 6 experiments ± s.e.m.).

Figure 6: Effect of LUV diameter on estimated proton permeability. Proton permeability was measured in LUV of different sizes (measured by DLS, see Table S2 (SI)) in the absence or presence of CL. n = 4-6 experiments, ± s.e.m.